NeuroImage: Clinical 32 (2021) 102863

Contents lists available at ScienceDirect

NeuroImage: Clinical

journal homepage: www.elsevier.com/locate/ynicl

White matter microstructural impairments in amyotrophic lateral sclerosis: A mean apparent propagator MRI study

Hua-Jun Chen [a,1,*], Chuanyin Zhan [a,1], Li-Min Cai [a,1], Jia-Hui Lin, Data curation, Formal analysis, Investigation, Writing – review & editing. [a,1], Min-Xiong Zhou [b,1], Zhang-Yu Zou [c,1], Xu-Feng Yao [b], Yan-Juan Lin [d,e,*]

[a] Department of Radiology, Fujian Medical University Union Hospital, Fuzhou 350001, China
[b] College of Medical Imaging, Shang Hai University of Medicine & Health Sciences, Shanghai 201318, China
[c] Department of Neurology, Fujian Medical University Union Hospital, Fuzhou 350001, China
[d] Department of Cardiovascular Surgery, Fujian Medical University Union Hospital, Fuzhou 350001, China
[e] Department of Nursing, Fujian Medical University Union Hospital, Fuzhou 350001, China

ARTICLE INFO

Keywords:
Amyotrophic lateral sclerosis
White matter
Mean apparent propagator
Diffusion weighted imaging
Corticospinal tract

ABSTRACT

Background: White matter (WM) impairment is a hallmark of amyotrophic lateral sclerosis (ALS). This study evaluated the capacity of mean apparent propagator magnetic resonance imaging (MAP-MRI) for detecting ALS-related WM alterations.

Methods: Diffusion images were obtained from 52 ALS patients and 51 controls. MAP-derived indices [return-to-origin/-axis/-plane probability (RTOP/RTAP/RTPP) and non-Gaussianity (NG)/perpendicular/parallel NG ($NG_{\perp}$/$NG_{||}$)] were computed. Measures from diffusion tensor/kurtosis imaging (DTI/DKI) and neurite orientation dispersion and density imaging (NODDI) were also obtained. Voxel-wise analysis (VBA) was performed to determine differences in these parameters. Relationship between MAP parameters and disease severity (assessed by the revised ALS Functional Rating Scale (ALSFRS-R)) was evaluated by Pearson's correlation analysis in a voxel-wise way. ALS patients were further divided into two subgroups: 29 with limb-only involvement and 23 with both bulbar and limb involvement. Subgroup analysis was then conducted to investigate diffusion parameter differences related to bulbar impairment.

Results: The VBA (with threshold of $P < 0.05$ after family-wise error correction (FWE)) showed that ALS patients had significantly decreased RTOP/RTAP/RTPP and NG/ $NG_{\perp}$/$NG_{||}$ in a set of WM areas, including the bilateral precentral gyrus, corona radiata, posterior limb of internal capsule, midbrain, middle corpus callosum, anterior corpus callosum, parahippocampal gyrus, and medulla. MAP-MRI had the capacity to capture WM damage in ALS, which was higher than DTI and similar to DKI/NODDI. RTOP/RTAP/NG/$NG_{\perp}$/$NG_{||}$ parameters, especially in the bilateral posterior limb of internal capsule and middle corpus callosum, were significantly correlated with ALSFRS-R (with threshold of FWE-corrected $P < 0.05$). The VBA (with FWE-corrected $P < 0.05$) revealed the significant RTAP reduction in subgroup with both bulbar and limb involvement, compared with those with limb-only involvement.

Conclusions: Microstructural impairments in corticospinal tract and corpus callosum represent the consistent characteristic of ALS. MAP-MRI could provide alternative measures depicting ALS-related WM alterations, complementary to the common diffusion imaging methods.

Abbreviations: WM, white matter; ALS, amyotrophic lateral sclerosis; MAP, mean apparent propagator; MRI, magnetic resonance imaging; DTI, diffusion tensor imaging; DKI, diffusion kurtosis imaging; NODDI, neurite orientation dispersion and density imaging; RTOP, return-to-origin probability; RTAP, return-to-axis probability; RTPP, return-to-plane probability; NG, non-Gaussianity; $NG_{\perp}$, perpendicular NG; $NG_{||}$, parallel NG; FA, fractional anisotropy; MD, mean diffusivity; RD, radial diffusivity; AD, axial diffusivity; MK, mean kurtosis; RK, radial kurtosis; AK, axial kurtosis; NDI, neurite density index; ODI, orientation dispersion index; ISO, isotropic compartment fraction; VBA, voxel-wise analysis; ALSFRS-R, revised ALS Functional Rating Scale; CST, corticospinal tract; PDF, probability density function; HCs, healthy controls.

* Corresponding authors at: Department of Radiology, Fujian Medical University Union Hospital, Fuzhou 350001, China (H.-J. Chen). Department of Cardiovascular Surgery, Fujian Medical University Union Hospital Fuzhou 350001, China (Y.-J. Lin).
E-mail addresses: chj0075@126.com (H.-J. Chen), fjxhlyj@163.com (Y.-J. Lin).
[1] These authors equally contributed to this work.

https://doi.org/10.1016/j.nicl.2021.102863
Received 28 March 2021; Received in revised form 8 October 2021; Accepted 18 October 2021
Available online 23 October 2021

1. Introduction

Amyotrophic lateral sclerosis (ALS) is a rare, progressive neurodegenerative disorder with unknown etiology and devastating effects that result in the loss of upper and lower motor neurons. Clinical manifestations of ALS include motor dysfunction (e.g., muscle weakness, muscle atrophy, and dysphagia) and cognitive and behavioral impairment (Hardiman et al., 2017). ALS progresses rapidly, leading to respiratory failure and ultimately the death of ALS patients due within 3 to 5 years of symptom onset (Hardiman et al., 2011). Unfortunately, there is currently no effective treatment available for ALS. Of note, previous studies have demonstrated that the modifications of white matter (WM) microstructure and function (e.g., the increase in axonal initial segment diameter and axonal ribosome numbers and altered axonal excitability (Iwai et al., 2016; Sasaki and Maruyama, 1992; Verheijen et al., 2014)) are early events implicated in the pathogenesis of ALS. Therefore, investigating the WM alteration related to ALS might offer novel insights and therapeutic targets for ALS treatment.

The impairment of WM integrity in ALS has been well documented. Neuropathological studies have identified ALS-related WM abnormalities, including axonal loss and demyelination in the corticospinal tract (CST) and spinal cord (Matsusue et al., 2007) and the accumulation of phosphorylated 43-kDA TAR DNA-binding protein (pTDP-43) in the CST, corpus callosum, and cingulum (Fatima et al., 2015). Neuroimaging studies have also provided evidence of WM impairment in ALS. At the macroscopic level, a *meta*-analysis conducted on voxel-based morphometry studies found volume losses in several WM tracts in ALS, including the CST, subcortical arcuate fibers, interhemispheric fibers, and projection fibers to the striatum and cortico-ponto-cerebellar tract (Chen et al., 2018). At the microscopic level, based on voxel-based analysis (VBA), diffusion tensor imaging (DTI) studies have reported ALS-related WM damage (as reflected by decreased fractional anisotropy (FA)) in several regions, involving the CST, corpus callosum, cingulum, and superior longitudinal fasciculus (Prudlo et al., 2012; Zhang et al., 2018). Furthermore, DTI studies examining voxel-based connectivity index and FA metric have shown aberrant WM connectivity in ALS that involved the CST and motor network (Ciccarelli et al., 2006; Verstraete et al., 2011).

However, DTI assumes that water molecule diffusion in the brain follows Gaussian distribution, weakening its capability to detect diffusion heterogeneity in brain tissue (Arab et al., 2018). Several additional diffusion magnetic resonance imaging (MRI) techniques, such as diffusion kurtosis imaging (DKI) and neurite orientation and dispersion density imaging (NODDI), further elaborated ALS-related WM microstructure alterations. For instance, a prior DKI study in ALS found abnormal WM microstructures (as reflected by decreased mean kurtosis (MK) and radial kurtosis (RK)) in the CST pathway and middle corpus callosum (Huang et al., 2020). Moreover, recent NODDI studies have detected ALS-related WM damage (as reflected by decreased neurite density index (NDI)) in the bilateral CST, corpus callosum, and frontotemporal-related tracts (Broad et al., 2019; Wen et al., 2019).

Quite recently, Özarslan et al. proposed an efficient, quantitative, and robust mathematical and physical framework, namely, mean apparent propagator (MAP) MRI, to model the three-dimensional *q*-space signal and transform it into diffusion propagators (Ozarslan et al., 2013). By measuring the probability density function (PDF) of spin displacement, MAP-MRI could provide useful measures in complex tissue microstructures (e.g., restrictions and multiple compartments) (Avram et al., 2016). In fact, it extends the diffusion signal analytically in the local DTI reference frame using a complete set of orthogonal basis functions (Ozarslan et al., 2013). It contributes to improve robustness to noise and immunity from signal confounds; and with scalar descriptors of the propagator, MAP-MRI can better quantify brain microstructural characteristics (Avram et al., 2016). The quantitative measures derived from MAP-MRI include zero-displacement probabilities, non-Gaussianity (NG), and propagator anisotropy, which are relevant to the tissue microstructural features such as cellularity and restrictions, diffusion heterogeneity, and the degree of anisotropy (Avram et al., 2016). Several studies have already investigated the application value of MAP-MRI. MAP-MRI provides a more comprehensive and sensitive brain microstructure characterization in healthy subjects (Avram et al., 2016; Fick et al., 2016). In addition, MAP-MRI has been demonstrated to provide sensitive detection of microstructural alterations in the brain due to multiple pathological conditions such as stroke (Brusini et al., 2016), Alzheimer's disease (Fick et al., 2017), and epilepsy (Ma et al., 2020).

In this study, we investigated the ALS-related WM microstructure alterations using MAP-MRI for the first time. This study had the following aims: 1) to evaluate the feasibility of MAP-MRI for capturing disrupted WM microstructures in ALS patients; 2) to compare the capability of MAP-MRI with conventional DTI, DKI, and NODDI for the detection of ALS-related WM damage; and 3) to examine the potential of MAP-MRI measures for monitoring the disease severity of ALS.

Table 1
Demographic and clinical characteristics of the study subjects.

	Healthy controls ($n = 51$)	ALS patients ($n = 52$)	*P* value*
Age (years)	52.8 ± 9.1	54.3 ± 10.7	0.434
Sex (female/male)	14/37	20/32	0.235
Education (years)	8.4 ± 3.1	7.6 ± 4.2	0.280
Site of onset (bulbar/limb)	–	9/43	–
Disease distribution clinically (bulbar and limb involvement/limb involvement only)	–	23/29	–
Diagnostic category (definite/probable/possible)	–	10/20/22	–
ALSFRS-R score	–	41.0 ± 6.0	–
Disease duration (months)	–	15.5 ± 14.5	–
Progression rate	–	0.58 ± 0.56	–

ALS, amyotrophic lateral sclerosis; ALSFRS-R, revised ALS Functional Rating Scale. The rate of disease progression was calculated using the equation: (48 - ALSFRS-R)/Disease duration. "-" denotes no data available. * indicates that the continuous and categorical variables were compared using a two-sample *t* test and chi-square test, respectively.

2. Methods

2.1. Subjects

The subjects in this study comprised a total of 103 patients, among which 52 had sporadic ALS and 51 were healthy controls (HCs). ALS was diagnosed using the El Escorial criteria [23], and the revised ALS Functional Rating Scale (ALSFRS-R) was used to assess the severity of disease. There were no significant differences in terms of age, gender, and education level between the ALS patient and control groups. Detailed clinical and demographic data are shown in Table 1. The following exclusion criteria were used: 1) other neuropsychiatric diseases (e.g., Parkinson's disease, Alzheimer's disease, epilepsy, schizophrenia, and depression); 2) taking psychotropic drugs; 3) suffering from other severe disorders (e.g., respiratory failure, cardiovascular diseases, malignant tumors); and 4) contraindications of MRI examination. This study was approved by the Research Ethics Committee of Fujian Medical University Union Hospital, and written informed consent was obtained from all subjects.

2.2. MRI data acquisition

Participants were scanned on a Siemens Prisma 3.0 T scanner with

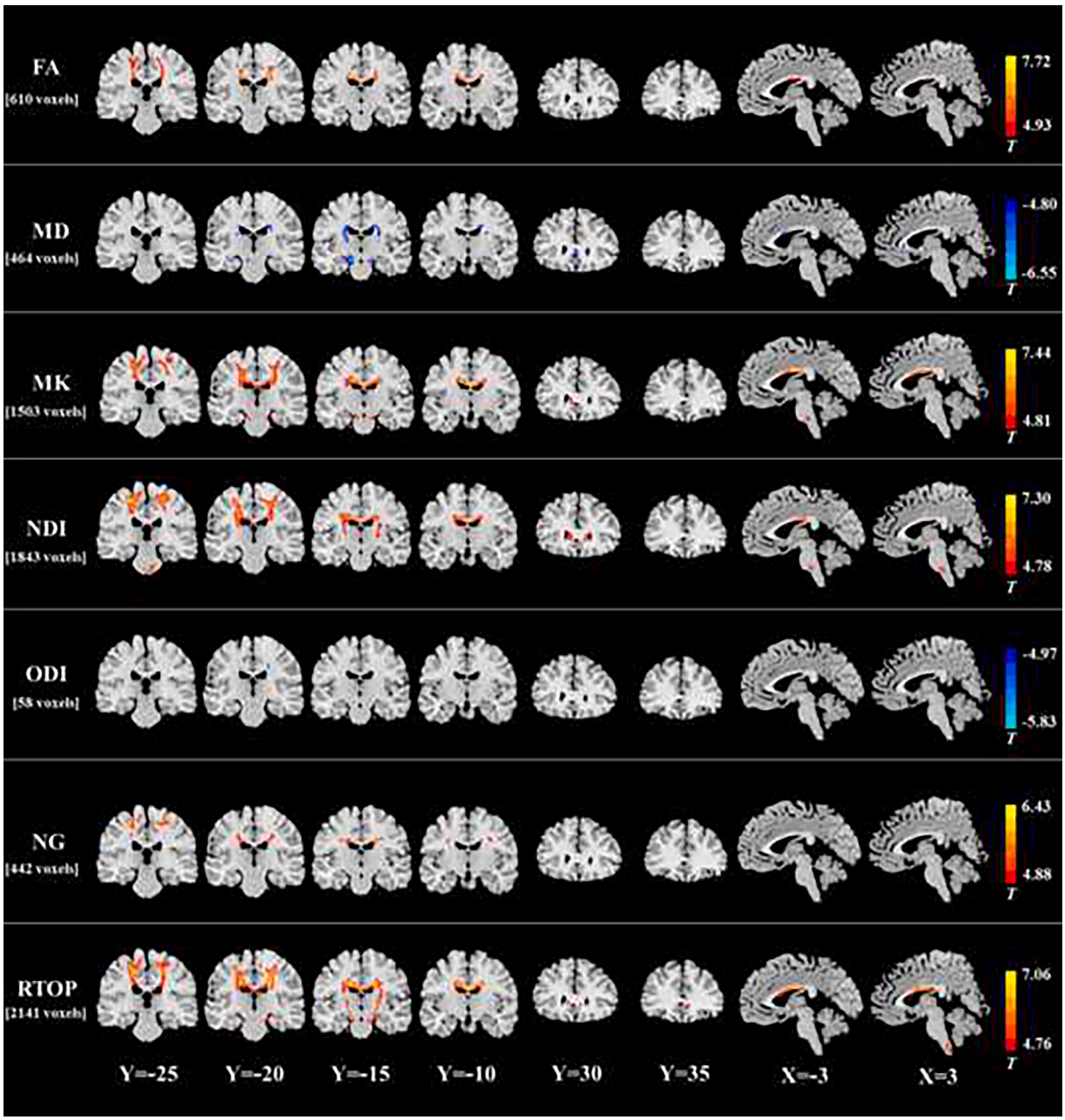

Fig. 1. White matter regions in the ALS group with significant decreases in FA, MK, NDI, NG, and RTOP and increases in MD and ODI. The spatial extent of WM area with altered diffusion measures is indicated by total voxel number. Left and right sides of the image respectively indicate the left and right hemisphere of brain.

64-channel head coil. Diffusion images were acquired with a spin-echo echo-planar imaging sequence, using a full *q*-space Cartesian grid sampling scheme, which has been applied in previous MAP-MRI studies (Jiang et al., 2021; Le et al., 2020; Mao et al., 2020). For each participant, 100 diffusion-weighted images were acquired at following *b*-values (direction number): 0 (2), 350 (6), 600 (12), 1000 (8), 1400 (6), 1650 (24), 2000 (24), 2700 (12), and 3000 (6) s/mm^2. The other sampling parameters were as follows: repetition time = 4000 ms; echo time = 72 ms; diffusion time parameters (Δ = 35 ms and δ = 15.9 ms); field of view = 220 mm × 220 mm; matrix = 110 × 110; slice thickness = 2 mm; slice number = 72 axial slices (gap = 0); isotropic resolution = 2 mm^3; slice acceleration factor = 2; inplane acceleration factor = 2; total scanning time = 429 s. The signal-to-noise ratio (SNR) of diffusion data, which was calculated according to reference (Kaufman et al., 1989), was 16.7 ~ 57.2 for *b*-value of 0 ~ 3000 s/mm^2.

2.3. Diffusion data processing

For each subject's data, the quantitative metrics from DTI (FA, mean diffusivity (MD), axial diffusivity (AD), and radial diffusivity (RD)), DKI (MK, axial kurtosis (AK), and RK), NODDI (NDI, orientation dispersion index (ODI), and isotropic component fraction (ISO)), and MAP (return-to-origin probability (RTOP), return-to-axis probability (RTAP), return-to-plane probability (RTPP), NG, perpendicular NG ($NG_{\perp}$), and parallel NG ($NG_{||}$)) models were simultaneously calculated using an in-house developed tool called NeuDiLab, which was based on Python 3.5 and open-resource projects previously validated (Mao et al., 2020). The processing pipeline included the following steps: 1) the skull was removed by BET from FSL (Jenkinson et al., 2012); 2) eddy current distortion and motion artifacts were corrected using the bneddy tool from DiffusionKit (Xie et al., 2016); 3) a 3D Gaussian filter was applied to diffusion data with a full width at half maximum (FWHM) at 3 mm to

increase SNR and reduce potential misregistration among diffusion data. The FWHM was set at 1.5 times of voxel size according to previous studies (Tabesh et al., 2011; Yan et al., 2014); 4) metrics of DTI, DKI, and MAP were estimated by algorithms from DIPY (Garyfallidis et al., 2014), and the NODDI model metrics were estimated by AMICO (Daducci et al., 2015). DTI metrics were calculated only on data points with *b*-values $\leq$ 1000 s/mm^2; whereas, other diffusion metrics were calculated with all acquired *b*-values.

2.4. Voxel-based analysis

The VBA was conducted to investigate the alterations in the DTI, DKI, NODDI, and MAP metrics between patients and HCs by using SPM12 (https://www.fil.ion.ucl.ac.uk/spm/), which implemented the general linear model. The normalization process adopted a two-step strategy based on *b*0 data: 1) A subject-specific template was first created by nonlinearly normalizing *b*0 data of all HCs to EPI MNI template in SPM, followed by average and Gaussian smoothing with FWHM = 6 mm; 2) *b*0 data of all subjects were normalized to the subject-specific template and the resulting deformation fields were applied to their corresponding quantitative metrics of all diffusion models. Finally, Gaussian smoothing was applied with FWHM = 6 mm. Between-group differences in the diffusion metrics were then determined by a two-sample *t*-test with the statistical threshold set at $P < 0.05$ after family-wise error correction. The covariates were age, gender, and education level. The VBA processes were confined to a WM mask, which was created by selecting a threshold of 0.2 on the averaged FA map of all subjects.

2.5. Correlation analysis

A Pearson's correlation analysis was conducted among ALS patients to evaluate the relationship between disease severity as assessed by an ALSFRS-R score and MAP metrics in a voxel-wise way. The covariates were age, gender, and education level. The correlation analysis was confined to the WM areas in which the significant between-group differences in diffusion metrics were found during VBA. The statistical threshold was set at a P value < 0.05 with family-wise error correction. Using the same procedures, the Pearson's correlation analyses were also conducted to investigate the relationship between disease severity and other diffusion metrics (see Supplementary Fig. 1).

2.6. Subgroup analysis

The ALS patients were further divided into two subgroups according to the disease clinical distribution: 29 with limb-only involvement and 23 with both bulbar and limb involvement. The scores on the three bulbar items in the ALSFRS-R (i.e. speech, sialorrhoea, and swallowing; a score of four per item indicating normal function) were used to define the presence of bulbar involvement. The VBA of DTI, DKI, NODDI, and MAP metrics between two subgroups were performed using the general linear model framework implemented in SPM12. The statistical threshold was set at $P < 0.05$ after family-wise error correction. The covariates were age, gender, and education level.

3. Results

Compared with HCs, ALS patients showed an extensive reduction of MAP metrics in a set of WM regions. The patients with ALS had decreased RTOP in the bilateral precentral gyrus, corona radiata, posterior limb of internal capsule, midbrain, middle corpus callosum, anterior corpus callosum, parahippocampal gyrus, and medulla (Fig. 1 and Table 2). In these WM areas, the MD/ODI increment or FA/MK/NDI/NG reduction was also observed in the ALS group. In fact, VBA revealed the greatest differences in RTOP (2141 voxels), followed in order by NDI (1843 voxels), MK (1503 voxels), FA (610 voxels), MD (464 voxels), NG (442 voxels), and ODI (58 voxels). No significant ISO difference was found between two groups.

Table 2
White matter regions with altered non-directional diffusion metrics in the ALS group.

Regions	Voxels	MNI coordinates			Peak *T*-value
		x	y	z	
FA reduction					
Bilateral precentral gyrus, corona radiata, and middle corpus callosum	600	−16	−16	34	7.72
Right middle occipital gyrus	10	32	−74	0	5.68
MD increment					
Left midbrain and parahippocampal gyrus	137	−10	−18	−16	−6.55
Right corona radiata and posterior limb of internal capsule	116	22	−18	32	−5.45
Left corona radiata and posterior limb of internal capsule	90	−24	−16	22	−5.61
Bilateral anterior corpus callosum	31	0	28	2	−5.53
Right midbrain	27	14	−14	−16	−5.38
Bilateral middle corpus callosum	20	−2	8	22	−5.24
Right parahippocampal gyrus	18	22	–32	−6	−5.04
Right anterior cingulate gyrus	15	6	34	−10	−5.57
Left anterior corpus callosum	10	−8	24	16	−5.21
MK reduction					
Bilateral precentral gyrus, corona radiata, and middle corpus callosum	1356	−2	−10	26	7.44
Left midbrain and pons	57	−12	−18	−20	6.49
Right midbrain and parahippocampal gyrus	52	12	−16	−20	6.00
Left anterior corpus callosum	21	−10	30	0	5.19
Pons	17	−4	−28	−42	5.68
NDI reduction					
Bilateral precentral gyrus, corona radiata, posterior limb of internal capsule, and middle corpus callosum, and right anterior corpus callosum	1678	−26	–22	54	7.30
Pons and medulla	98	4	−26	−44	6.33
Left anterior corpus callosum	67	−12	30	4	5.33
ODI increment					
Right corona radiata	24	20	−18	36	−5.83
Left corona radiata	22	−18	−18	34	−5.76
Left middle corpus callosum	12	−6	−12	28	−5.66
NG reduction					
Left precentral gyrus and corona radiata	249	−10	−26	66	6.43
Right corona radiata	112	18	−16	32	6.02
Right precentral gyrus	81	26	−24	62	6.05
RTOP reduction					
Bilateral precentral gyrus, corona radiata, and middle corpus callosum, and right posterior limb of internal capsule, midbrain, and parahippocampal gyrus	1949	4	−4	24	7.06
Left posterior limb of internal capsule, midbrain, and parahippocampal gyrus	113	−14	−18	−18	6.06
Medulla	35	0	−42	−64	6.39
Right anterior corpus callosum	31	10	32	−2	5.12
Left anterior corpus callosum	13	−10	32	0	5.01

In the between-group comparison on radially directional measurements (Fig. 2 and Table 3), we found that RTAP reduction was the most extensive (1957 voxels), followed in order by $NG_{\perp}$ decrease (1684 voxels), RK decrease (1405 voxels), and RD increase (762 voxels) in ALS patients. The spatial distribution of WM areas with altered radially directional metrics was highly similar to those of areas with RTOP/NDI/MK/FA/MD/NG/ODI changes.

In the between-group comparison on the axially directional

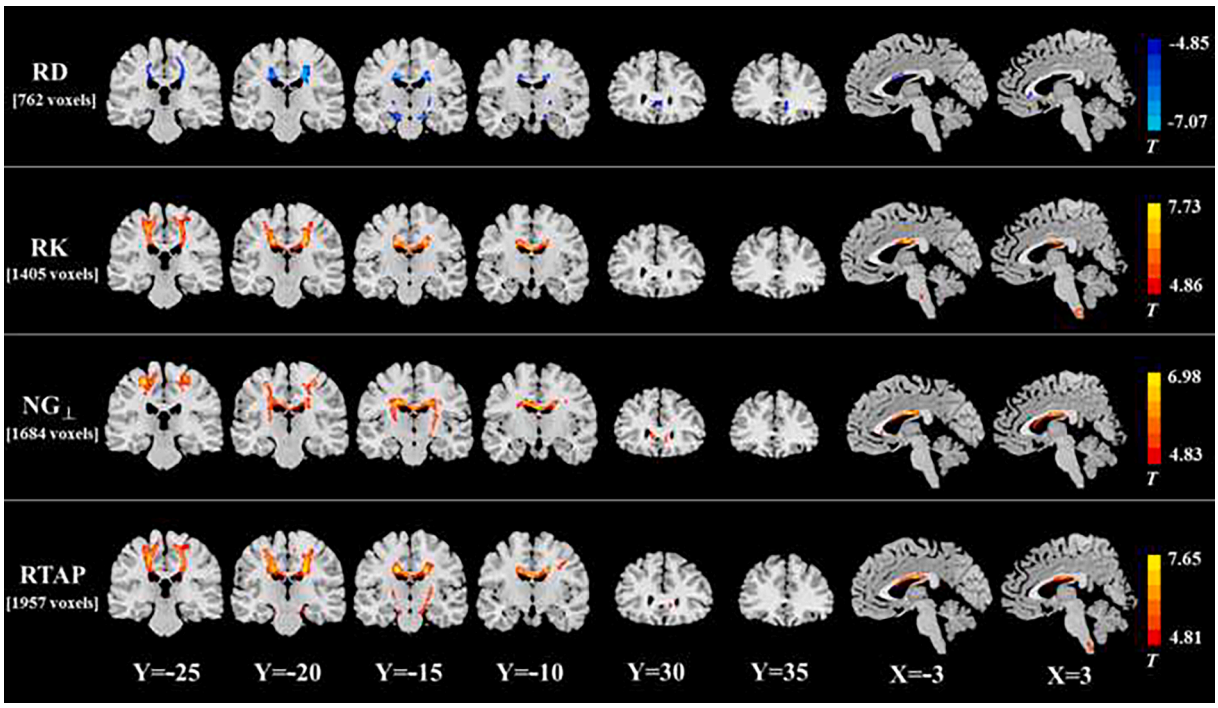

Fig. 2. White matter regions in the ALS group with significant increase in RD and decreases in RK, $NG_{\perp}$, and RTAP. The spatial extent of WM area with altered diffusion measures is indicated by total voxel number. Left and right sides of the image respectively indicate the left and right hemisphere of brain.

measurements (Fig. 3 and Table 4), we found that WM areas with $NG_{||}$ reduction (148 voxels) were more extensive than those with AK decrease (73 voxels) or RTPP decrease (52 voxels) in the ALS group. The spatial distribution of WM areas with altered axially directional metrics was similar to those of areas with RTOP/NDI/MK/FA/MD/NG/ODI changes, but their spatial extent was dramatically reduced. No significant AD difference was found between two groups.

Figure 4 shows the results of voxel-wise correlation analysis among the patients. The areas in which RTOP was positively correlated with ALSFRS-R score included 509 voxels in WM and involved the left precentral gyrus, left corona radiata, and bilateral posterior limb of internal capsule and middle corpus callosum. The WM areas in which RTAP was correlated with ALSFRS-R score showed highly similar spatial distribution and were less extensive (384 voxels). There was no WM area whose RTPP value was found to be significantly correlated with ALSFRS-R score. The $NG_{\perp}$ in the bilateral posterior limb of internal capsule and middle corpus callosum (513 voxels) was positively correlated with ALSFRS-R score, whereas the WM areas in which $NG/NG_{||}$ (91 and 31 voxels, respectively) was correlated with ALSFRS-R score were much less extensive. In addition, in several WM areas, FA, MK, RK, and NDI were found to be positively correlated with ALSFRS-R score, while MD and RD were observed to be negatively correlated with ALSFRS-R score (Supplementary Fig. 1). These WM areas primarily involved bilateral corona radiata, posterior limb of internal capsule, and midbrain (Supplementary Fig. 1).

In the subgroup analysis using the VBA, the significant RTAP reduction was found in left posterior limb of internal capsule in the ALS patients with both bulbar and limb involvement, compared with those with limb-only involvement (Fig. 5). No significant differences in the other DTI, DKI, NODDI, and MAP metrics were found between the two ALS subgroups, after family-wise error correction for multiple comparisons.

4. Discussion

In this study, we explored the performance of MAP-MRI in detecting ALS-related WM alterations and compared it with other diffusion models such as conventional DTI, DKI, and NODDI. Our main findings can be summarized as follows. First, ALS patients showed extensive alteration of non-directional MAP metrics (as reflected by decreased RTOP and NG) in a set of WM areas involving several motor-related brain regions (including the bilateral precentral gyrus, corona radiata, posterior limb of internal capsule, midbrain, medulla, and middle corpus callosum) and cognition-related regions (including the anterior corpus callosum and parahippocampal gyrus). Second, WM regions with decreased radially directional MAP metrics showed a similar distribution to that with RTOP and NG changes; the spatial distribution of WM regions with decreased axially directional MAP metrics was also similar to the distribution of RTOP and NG changes, but the spatial extent was dramatically reduced. Third, MAP-MRI showed the robust capacity to capture WM damage, which was higher than that of the conventional DTI and similar to that of other advanced diffusion models (such as DKI and NODDI), regardless of the directional or non-directional metrics used. Fourth, voxel-wise correlation analysis showed that MAP metrics were correlated with disease severity (as represented by ALSFRS-R score) with various degrees. Fifth, the significant WM abnormality related to bulbar impairment was only detected by MAP measure (i.e. RTAP). Taken together, MAP-MRI can offer complementary information for ALS-related WM damage to other diffusion models, which might provide novel insights on the pathogenesis of ALS.

The specific neuropathological substrate that underlies ALS-related WM damage is linked to multiple factors such as axon and myelin. As previous pathological studies have found, ALS is a progressive axonopathy. Distal axonal degeneration is found at the very early stage of ALS, prior to symptom onset (Fischer et al., 2004; Moloney et al., 2014). Several ALS genes (e.g., dynactin 1 and tublin 4A) encode cytoskeletal proteins important for the maintenance of axonal transport and integrity (Pensato et al., 2015; Puls et al., 2003); mutations in these genes might contribute to the axonal disruption. On the other hand, glial cells (e.g., astrocytes and oligodendrocytes) are critical for preserving axonal integrity (Edgar and Nave, 2009). For instance, astrocytes participate in the differentiation and maturation of oligodendrocytes (Li et al., 2016); oligodendrocytes generate and maintain the myelin sheath around the axon, ensuring the conduction of action potentials (Philips and

Table 3
White matter regions with altered radially directional diffusion metrics in the ALS group.

Regions	Voxels	MNI coordinates			Peak *T*-value
		x	y	z	
RD increment					
Right precentral gyrus and corona radiata	279	20	−18	34	−7.07
Left precentral gyrus and corona radiata	195	−16	−16	36	−6.77
Left midbrain and parahippocampal gyrus	88	−14	−16	−14	−6.19
Bilateral anterior cingulate gyrus and anterior corpus callosum	78	8	36	−6	−5.49
Right midbrain	42	16	−14	−14	−5.73
Right posterior limb of internal capsule	26	22	−12	2	−5.82
Bilateral middle corpus callosum	26	−4	6	24	−5.36
Left parahippocampal gyrus	18	–22	–32	−6	−5.27
Left posterior limb of internal capsule	10	–22	−16	2	−5.39
RK reduction					
Bilateral precentral gyrus, corona radiata, and middle corpus callosum	1328	−4	−10	26	7.73
Medulla	61	0	−40	−62	7.39
Pons	16	−4	−28	−42	5.57
$NG_{\perp}$ reduction					
Left precentral gyrus, and bilateral corona radiata, posterior limb of internal capsule, and middle corpus callosum	1440	−2	−10	26	6.98
Right precentral gyrus and corona radiata	140	28	−20	54	6.20
Right anterior corpus callosum	43	10	32	−4	5.71
Left anterior corpus callosum	36	−8	30	2	5.53
Right anterior corpus callosum	15	12	22	14	5.21
Right midbrain	10	20	−16	−10	5.67
RTAP reduction					
Bilateral precentral gyrus, corona radiata, and middle corpus callosum	1711	−16	−16	34	7.65
Right midbrain, parahippocampal gyrus, and posterior limb of internal capsule	121	24	−14	6	6.32
Left midbrain and posterior limb of internal capsule	68	–22	−16	4	5.97
Medulla	39	0	−40	−62	6.75
Right anterior corpus callosum	18	10	32	−2	5.12

Rothstein, 2014). Astrocyte and oligodendrocyte dysfunction in ALS has been well documented (Philips and Rothstein, 2014), which might lead to the axonal demyelination that has been described in ALS (Hayashi et al., 1986; Smith, 1960). Our study determined that ALS patients had abnormalities in directional MAP metrics, which was in accordance with neuropathological findings. Directional diffusion metrics, including parallel indices such as AD, AK, RTPP, and $NG_{||}$ and perpendicular metrics such as RD, RK, RTAP, and $NG_{\perp}$, respectively reflected the presence of restrictive barriers or heterogeneous diffusion in the axial and radial orientation, which are associated with axonal integrity and myelination (Andica et al., 2019; Avram et al., 2016). Changes in directional MAP metrics induced by ALS could therefore provide distinctive WM biomarkers for axonal loss and demyelination.

We observed impaired WM microstructures (as reflected by decreased RTOP and NG) in the ALS group in several brain areas, including motor as well as cognitive regions. WM damage in motor regions in ALS primarily involved the CST pathway (including the bilateral precentral gyrus, corona radiata, posterior limb of internal capsule, midbrain, and medulla) and middle corpus callosum, which was in line with previous diffusion and structural MRI studies (Huang et al., 2020; Ishaque et al., 2019; Wen et al., 2019; Yamauchi et al., 1995; Zhang et al., 2018). The CST transmits motor impulses from the motor and premotor cortices to the spinal cord, thereby mediating voluntary distal movements (Welniarz et al., 2017); and the middle corpus callosum connects homologous cortical regions relevant for motor function such as precentral frontal regions and parietal lobes (Catani and Thiebaut de Schotten, 2008), which are involved in the control and coordination of bilateral movements (Richmond and Fling, 2019). WM damage in these motor regions might cause the delay or disruption of motor impulse conduction, which is a potential mechanism of motor dysfunction in ALS. Additionally, in accordance with previous studies (Abrahams et al., 2005; Chapman et al., 2014), we also observed WM microstructural alterations in several cognition-related regions such as the anterior corpus callosum and parahippocampal gyrus. The anterior corpus callosum aids in the inter-hemispheric integration of cognitive information by connecting the prefrontal and orbitofrontal areas (Catani and Thiebaut de Schotten, 2008); the parahippocampal gyrus is part of a large network connecting frontal, parietal, and temporal cortices, which is closely linked to many cognitive processes (e.g., visuospatial processing and episodic memory) (Aminoff et al., 2013). Thus, it is speculated that WM abnormalities in these cognition-related regions might be specifically associated with the presence of well-described cognitive impairments in ALS (Hardiman et al., 2017). A future study which directly examine the association between ALS-related WM impairment and cognitive dysfunction is recommended to verify this speculation.

In keeping with previous studies (Bao et al., 2018; Schuster et al., 2016), our findings revealed that DTI could detect ALS-related WM microstructure alterations, particularly RD (which is considered as the most sensitive DTI metric and reflects WM demyelination). Furthermore, our results agreed with preceding DKI research in ALS (Huang et al., 2020), which has demonstrated that DKI (as a mathematical extension of DTI quantifying non-Gaussian diffusion) provides a better characterization of WM abnormalities in ALS, relative to DTI. Consistent with prior NODDI studies in ALS (Broad et al., 2019; Wen et al., 2019), our results also suggested that NODDI can offer higher sensitivity and greater tissue specificity than DTI in detecting WM abnormalities. More importantly, compared with conventional DTI and other advanced diffusion models (DKI/NODDI), our findings revealed that MAP-MRI could provide additional indicators to effectively depict ALS-related WM alterations. Owing to the inherent limitation of DTI on the assumption of Gaussian spin displacement distribution, its ability to describe intricate tissue microanatomy is weakened, while MAP-MRI efficiently measures the PDF of spin displacements and quantifies useful metrics of this PDF, thereby facilitating the indication of multiple-compartmental and restricted diffusion in complex tissue microstructures (Avram et al., 2016). Thus, it was not unexpected that the sensitivity of MAP was higher than that of DTI. Furthermore, in comparison with DKI, MAP-MRI might offer sensitive indicators to comprehensively characterize WM pathological alterations such as axonal loss and demyelination. For instance, axonal loss in ALS has been validated, but that was rarely captured by the parallel diffusion metric (AK) derived from DKI; while ALS patients showed a more extensive distribution of WM regions with altered axial MAP metrics (i.e., $NG_{||}$ and RTPP), indicating that axial MAP metrics may detect axonal damage with higher capability. In addition, it seemed that MAP-MRI detected a broader range of ALS-related WM damage than NODDI, suggesting that at least MAP-MRI might have the potential similar to the NODDI in clinical application.

In consistence with previous report that the extent of WM impairment is associated with clinical involvement in ALS (Broad et al., 2019), we found the more widespread RTAP reduction in the subgroup with both limb and bulbar involvement compared to those with limb involvement alone. Thus, our findings also suggested the potential of MAP measurements for assessing the effect of ALS disease heterogeneity on WM microstructures. On the other hand, no significant difference related to bulbar impairment was observed in other diffusion parameters (e.g. NODDI metrics), which didn't keep in line with previous studies (Broad et al., 2019). This discrepancy may be due to the differences in

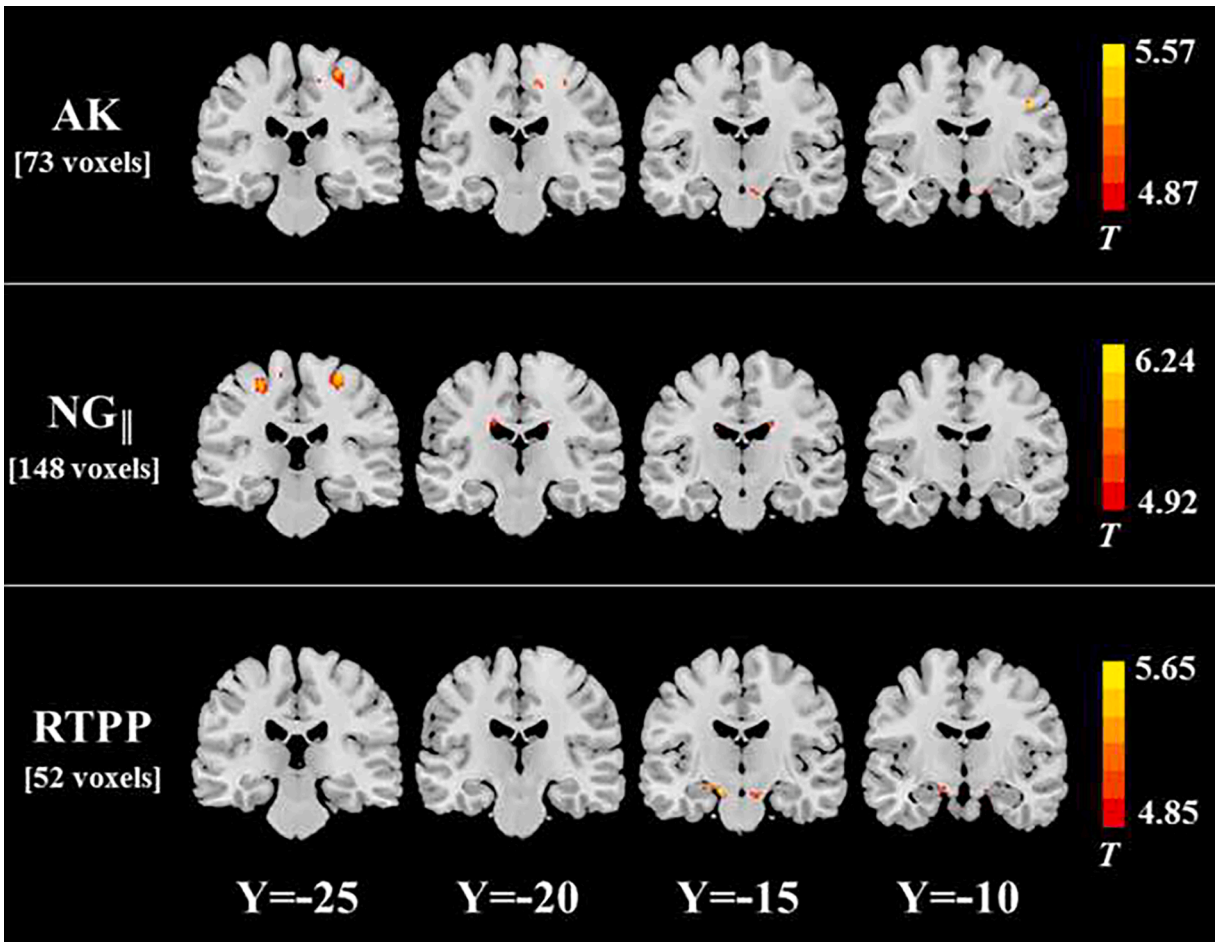

Fig. 3. White matter regions in the ALS group with significant decreases in AK, $NG_{||}$, and RTPP. The spatial extent of WM area with altered diffusion measures is indicated by total voxel number. Left and right sides of the image respectively indicate the left and right hemisphere of brain.

Table 4
White matter regions with altered axially directional diffusion metrics in the ALS group.

Regions	Voxels	MNI coordinates			Peak *T*-value
		x	y	z	
AK reduction					
Right precentral gyrus	34	26	−24	62	5.39
Right precentral gyrus	14	10	−22	56	5.19
Right precentral gyrus	13	44	−10	40	5.57
Right midbrain	12	8	−14	−20	5.15
$NG_{||}$ reduction					
Left precentral gyrus	46	−12	−26	66	6.24
Right precentral gyrus	35	28	−24	62	5.97
Left precentral gyrus	34	−26	−24	58	5.90
Left middle corpus callosum	17	−18	−20	32	5.43
Right middle corpus callosum	16	18	−16	32	5.51
RTPP reduction					
Left midbrain and parahippocampal gyrus	39	−14	−12	−16	5.65
Right midbrain	13	8	−14	−18	5.19

the sample collection and MRI data acquisition and processing between the current and previous diffusion studies.

This study had several limitations. First, due to the limited sample size, further research with a larger set of subjects is necessary to validate our results. Second, the cognitive function in ALS patients was not evaluated, hindering identification of the relationship between distinctive cognitive dysfunctions and the impaired integrity of specific WM regions. Third, in the acquisition protocol for MAP-MRI, the future studies could evaluate a better distribution of the gradient sampling, since the higher *b*-values are likely to indicate lower SNR which was not compensated by the denser sampling in this study. Fourth, in consideration of clinical feasibility (e.g. the relatively short period for MRI scanning), the diffusion acquisition protocol employed in this study was primarily designed towards the application of MAP-MRI, but was not the most optimal for other diffusion models (e.g. NODDI (Zhang et al., 2012)). The risk for performance underestimation of these diffusion models should be evaluated in the future study. Fifth, VBA method was applied in this study. Whereas, another method, called tract-based spatial statistics (TBSS), could be considered for voxel-wise group comparison of diffusion parametric maps especially when only white matter is included in the analysis, since its improved sensitivity and objectivity of the comparison and the obviation of spatial smoothing for diffusion data (Smith et al., 2006). Sixth, in data processing step, we applied Gaussian filter to improve fitting result of diffusion model, but it may also introduce slight smoothing effect. The advanced filters that can preserve more image details could be recommended in the future study (Glasser et al., 2013). Finally, as a limitation of cross-sectional study design, we did not perform the longitudinal investigation about how MAP-MRI metrics change over time.

In conclusion, our findings suggested that WM microstructural impairment, especially in the CST pathway and corpus callosum, represents the consistent characteristic of ALS and may be responsible for the disease progression. MAP-MRI could provide alternative measures depicting ALS-related WM alterations, complementary to the common diffusion imaging methods.

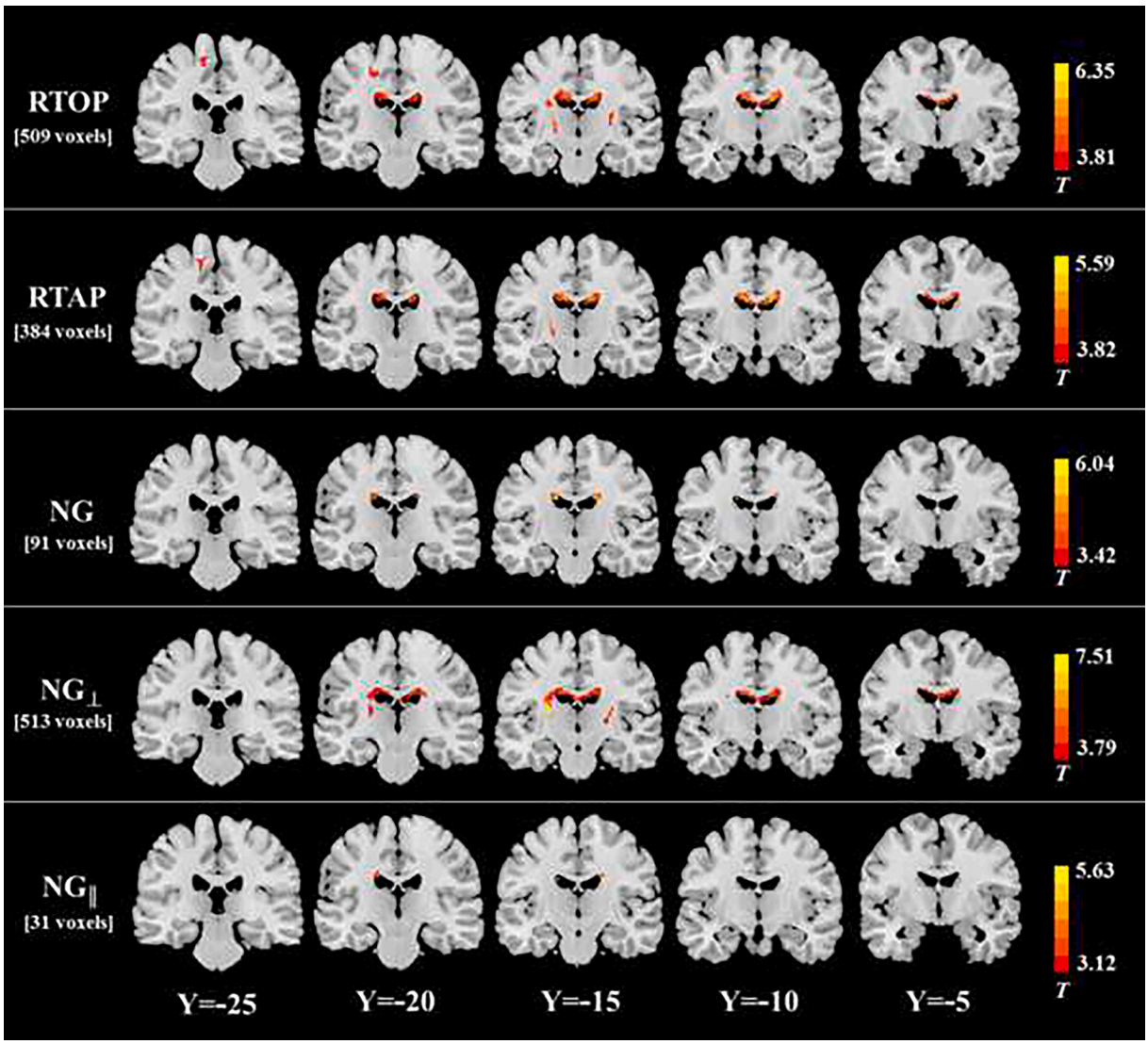

Fig. 4. The correlation between mean apparent propagator metrics and ALS disease severity indicated by ALSFRS-R score. The spatial extent of WM area in which MAP metrics are correlated with ALSFRS-R score is indicated by total voxel number. Left and right sides of the image respectively indicate the left and right hemisphere of brain.

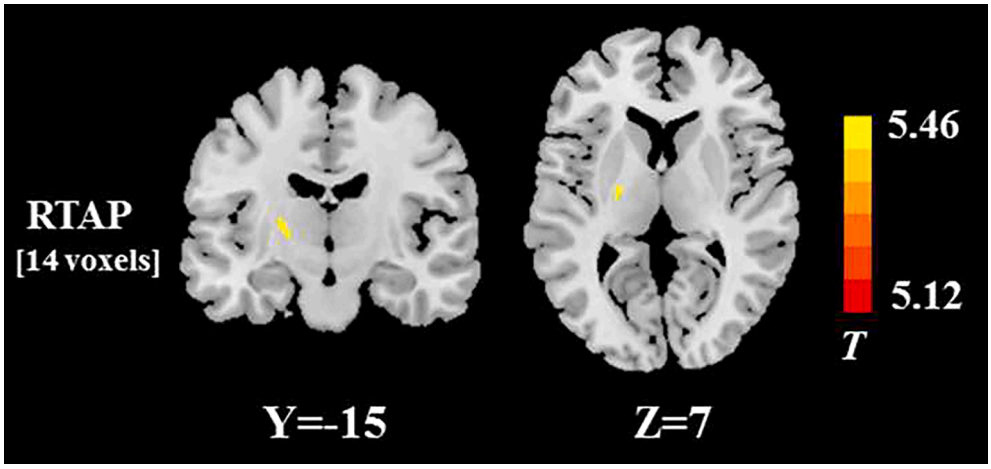

Fig. 5. White matter regions with the significant RTAP difference between two ALS subgroups stratified according to the presence or absence of bulbar involvement. The spatial extent of WM area is indicated by total voxel number. Left and right sides of the image respectively indicate the left and right hemisphere of brain.

Funding

This work was supported by grants from the National Natural Science Foundation of China (No. 82071900, 81671271 and 81974199), Fujian Province Natural Science Foundation (No. 2021J01754), and Fujian Province Joint Funds for the Innovation of Science and Technology (No. 2019Y9067).

CRediT authorship contribution statement

Hua-Jun Chen: Conceptualization, Data curation, Formal analysis, Funding acquisition, Investigation, Methodology, Project administration, Supervision, Validation, Writing – original draft, Writing – review & editing. **Chuanyin Zhan:** Data curation, Formal analysis, Funding acquisition, Writing – original draft, Writing – review & editing. **Li-Min Cai:** Data curation, Formal analysis, Investigation, Writing – review & editing. **Jia-Hui Lin:** Data curation, Formal analysis, Investigation, Writing – review & editing. **Min-Xiong Zhou:** Data curation, Formal analysis, Writing – original draft, Writing – review & editing. **Zhang-Yu Zou:** Data curation, Formal analysis, Writing – review & editing. **Xu-Feng Yao:** Data curation, Formal analysis. **Yan-Juan Lin:** Conceptualization, Data curation, Formal analysis, Investigation, Supervision, Writing – original draft, Writing – review & editing.

Declaration of Competing Interest

The authors declare that they have no known competing financial interests or personal relationships that could have appeared to influence the work reported in this paper.

Acknowledgements

The authors would like to thank all the participants who contributed to this study.

Appendix A. Supplementary data

Supplementary data to this article can be found online at https://doi.org/10.1016/j.nicl.2021.102863.

References

Abrahams, S., Goldstein, L.H., Suckling, J., Ng, V., Simmons, A., Chitnis, X., Atkins, L., Williams, S.C.R., Leigh, P.N., 2005. Frontotemporal white matter changes in amyotrophic lateral sclerosis. J. Neurol. 252 (3), 321–331.

Aminoff, E.M., Kveraga, K., Bar, M., 2013. The role of the parahippocampal cortex in cognition. Trends Cogn. Sci. 17 (8), 379–390.

Andica, C., Kamagata, K., Hatano, T., Saito, Y., Ogaki, K., Hattori, N., Aoki, S., 2019. MR biomarkers of degenerative brain disorders derived from diffusion imaging. J. Magn. Reson. Imaging 52 (6), 1620–1636.

Arab, A., Wojna-Pelczar, A., Khairnar, A., Szabó, N., Ruda-Kucerova, J., 2018. Principles of diffusion kurtosis imaging and its role in early diagnosis of neurodegenerative disorders. Brain Res. Bull. 139, 91–98.

Avram, A.V., Sarlls, J.E., Barnett, A.S., Ozarslan, E., Thomas, C., Irfanoglu, M.O., Hutchinson, E., Pierpaoli, C., Basser, P.J., 2016. Clinical feasibility of using mean apparent propagator (MAP) MRI to characterize brain tissue microstructure. NeuroImage 127, 422–434.

Bao, Y., Yang, L., Chen, Y., Zhang, B., Li, H., Tang, W., Geng, D., Li, Y., 2018. Radial diffusivity as an imaging biomarker for early diagnosis of non-demented amyotrophic lateral sclerosis. Eur. Radiol. 28 (12), 4940–4948.

Broad, R.J., Gabel, M.C., Dowell, N.G., Schwartzman, D.J., Seth, A.K., Zhang, H., Alexander, D.C., Cercignani, M., Leigh, P.N., 2019. Neurite orientation and dispersion density imaging (NODDI) detects cortical and corticospinal tract degeneration in ALS. J. Neurol. Neurosurg. Psychiatry 90 (4), 404–411.

Brusini, L., Obertino, S., Galazzo, I.B., Zucchelli, M., Krueger, G., Granziera, C., Menegaz, G., 2016. Ensemble average propagator-based detection of microstructural alterations after stroke. Int. J. Comput. Assist. Radiol. Surg. 11 (9), 1585–1597.

Catani, M., Thiebaut de Schotten, M., 2008. A diffusion tensor imaging tractography atlas for virtual in vivo dissections. Cortex 44 (8), 1105–1132.

Chapman, M.C., Jelsone-Swain, L., Johnson, T.D., Gruis, K.L., Welsh, R.C., 2014. Diffusion tensor MRI of the corpus callosum in amyotrophic lateral sclerosis. J. Magn. Reson. Imaging 39 (3), 641–647.

Chen, G., Zhou, B., Zhu, H., Kuang, W., Bi, F., Ai, H., Gu, Z., Huang, X., Lui, S.u., Gong, Q., 2018. White matter volume loss in amyotrophic lateral sclerosis: a meta-analysis of voxel-based morphometry studies. Prog. Neuro-Psychopharmacol. Biol. Psychiatry 83, 110–117.

Ciccarelli, O., Behrens, T.E., Altmann, D.R., Orrell, R.W., Howard, R.S., Johansen-Berg, H., Miller, D.H., Matthews, P.M., Thompson, A.J., 2006. Probabilistic diffusion tractography: a potential tool to assess the rate of disease progression in amyotrophic lateral sclerosis. Brain 129, 1859–1871.

Daducci, A., Canales-Rodríguez, E.J., Zhang, H., Dyrby, T.B., Alexander, D.C., Thiran, J.-P., 2015. Accelerated microstructure imaging via convex optimization (AMICO) from diffusion MRI data. Neuroimage 105, 32–44.

Edgar, J.M., Nave, K.-A., 2009. The role of CNS glia in preserving axon function. Curr. Opin. Neurobiol. 19 (5), 498–504.

Fatima, M., Tan, R., Halliday, G.M., Kril, J.J., 2015. Spread of pathology in amyotrophic lateral sclerosis: assessment of phosphorylated TDP-43 along axonal pathways. Acta Neuropathol. Commun. 3 (1) https://doi.org/10.1186/s40478-015-0226-y.

Fick, R.H.J., Daianu, M., Pizzolato, M., Wassermann, D., Jacobs, R.E., Thompson, P.M., Town, T., Deriche, R., 2017. Comparison of Biomarkers in Transgenic Alzheimer Rats Using Multi-Shell Diffusion MRI. In: Fuster, A., Ghosh, A., Kaden, E., Rathi, Y., Reisert, M. (Eds.), Computational Diffusion MRI. Springer International Publishing, Cham, pp. 187–199.

Fick, R.H.J., Wassermann, D., Caruyer, E., Deriche, R., 2016. MAPL: Tissue microstructure estimation using Laplacian-regularized MAP-MRI and its application to HCP data. NeuroImage 134, 365–385.

Fischer, L.R., Culver, D.G., Tennant, P., Davis, A.A., Wang, M., Castellano-Sanchez, A., Khan, J., Polak, M.A., Glass, J.D., 2004. Amyotrophic lateral sclerosis is a distal axonopathy: evidence in mice and man. Exp. Neurol. 185 (2), 232–240.

Garyfallidis, E., Brett, M., Amirbekian, B., Rokem, A., van der Walt, S., Descoteaux, M., Nimmo-Smith, I., Dipy, C., 2014. Dipy, a library for the analysis of diffusion MRI data. Front. Neuroinform. 8, 8.

Glasser, M.F., Sotiropoulos, S.N., Wilson, J.A., Coalson, T.S., Fischl, B., Andersson, J.L., Xu, J., Jbabdi, S., Webster, M., Polimeni, J.R., Van Essen, D.C., Jenkinson, M., 2013. The minimal preprocessing pipelines for the human connectome project. Neuroimage 80, 105–124.

Hardiman, O., Al-Chalabi, A., Chio, A., Corr, E.M., Logroscino, G., Robberecht, W., Shaw, P.J., Simmons, Z., van den Berg, L.H., 2017. Amyotrophic lateral sclerosis. Nat. Rev. Dis. Primers 3, 17071.

Hardiman, O., van den Berg, L.H., Kiernan, M.C., 2011. Clinical diagnosis and management of amyotrophic lateral sclerosis. Nat. Rev. Neurol. 7 (11), 639–649.

Hayashi, Y., Nagashima, K., Urano, Y., Iwata, M., 1986. Spinocerebellar degeneration with prominent involvement of the motor neuron system: autopsy report of a sporadic case. Acta Neuropathol. 70 (1), 82–85.

Huang, N.-X., Zou, Z.-Y., Xue, Y.-J., Chen, H.-J., 2020. Abnormal cerebral microstructures revealed by diffusion kurtosis imaging in amyotrophic lateral sclerosis. J. Magn. Reson. Imaging 51 (2), 554–562.

Ishaque, A., Mah, D., Seres, P., Luk, C., Johnston, W., Chenji, S., Beaulieu, C., Yang, Y.-H., Kalra, S., 2019. Corticospinal tract degeneration in ALS unmasked in T1-weighted images using texture analysis. Hum. Brain Mapp. 40 (4), 1174–1183.

Iwai, Y., Shibuya, K., Misawa, S., Sekiguchi, Y., Watanabe, K., Amino, H., Kuwabara, S., Phillips, W.D., 2016. Axonal dysfunction precedes motor neuronal death in amyotrophic lateral sclerosis. PLoS One 11 (7), e0158596. https://doi.org/10.1371/journal.pone.0158596.

Jenkinson, M., Beckmann, C.F., Behrens, T.E.J., Woolrich, M.W., Smith, S.M., 2012. Fsl. Neuroimage 62 (2), 782–790.

Jiang, R., Jiang, S., Song, S., Wei, X., Deng, K., Zhang, Z., Xue, Y., 2021. Laplacian-regularized mean apparent propagator-MRI in evaluating Corticospinal tract injury in patients with brain Glioma. Korean J Radiol 22 (5), 759. https://doi.org/10.3348/kjr.2020.0949.

Kaufman, L., Kramer, D.M., Crooks, L.E., Ortendahl, D.A., 1989. Measuring signal-to-noise ratios in MR imaging. Radiology 173 (1), 265–267.

Le, H., Zeng, W., Zhang, H., Li, J., Wu, X., Xie, M., Yan, X., Zhou, M., Zhang, H., Wang, M., Hong, G., Shen, J., 2020. Mean apparent propagator MRI is better than conventional diffusion tensor imaging for the evaluation of Parkinson's disease: a prospective pilot study. Front. Aging Neurosci. 12, 563595.

Li, J., Zhang, L., Chu, Y., Namaka, M., Deng, B., Kong, J., Bi, X., 2016. Astrocytes in oligodendrocyte lineage development and white matter pathology. Front. Cell. Neurosci. 10, 119.

Ma, K., Zhang, X., Zhang, H., Yan, X., Gao, A., Song, C., Wang, S., Lian, Y., Cheng, J., 2020. Mean apparent propagator-MRI: a new diffusion model which improves temporal lobe epilepsy lateralization. Eur. J. Radiol. 126, 108914. https://doi.org/10.1016/j.ejrad.2020.108914.

Mao, J., Zeng, W., Zhang, Q., Yang, Z., Yan, X., Zhang, H., Wang, M., Yang, G., Zhou, M., Shen, J., 2020. Differentiation between high-grade gliomas and solitary brain metastases: a comparison of five diffusion-weighted MRI models. BMC Med. Imaging 20, 124.

Matsusue, E., Sugihara, S., Fujii, S., Kinoshita, T., Nakano, T., Ohama, E., Ogawa, T., 2007. Cerebral cortical and white matter lesions in amyotrophic lateral sclerosis with dementia: correlation with MR and pathologic examinations. Am. J. Neuroradiol. 28 (8), 1505–1510.

Moloney, E.B., de Winter, F., Verhaagen, J., 2014. ALS as a distal axonopathy: molecular mechanisms affecting neuromuscular junction stability in the presymptomatic stages of the disease. Front. Neurosci. 8, 252.

Ozarslan, E., Koay, C.G., Shepherd, T.M., Komlosh, M.E., İrfanoğlu, M.O., Pierpaoli, C., Basser, P.J., 2013. Mean apparent propagator (MAP) MRI: a novel diffusion imaging method for mapping tissue microstructure. NeuroImage 78, 16–32.

Pensato, V., Tiloca, C., Corrado, L., Bertolin, C., Sardone, V., Del Bo, R., Calini, D., Mandrioli, J., Lauria, G., Mazzini, L., Querin, G., Ceroni, M., Cantello, R., Corti, S., Castellotti, B., Soldà, G., Duga, S., Comi, G.P., Cereda, C., Sorarù, G., D'Alfonso, S., Taroni, F., Shaw, C.E., Landers, J.E., Ticozzi, N., Ratti, A., Gellera, C., Silani, V., 2015. TUBA4A gene analysis in sporadic amyotrophic lateral sclerosis: identification of novel mutations. J. Neurol. 262 (5), 1376–1378.

Philips, T., Rothstein, J.D., 2014. Glial cells in amyotrophic lateral sclerosis. Exp. Neurol. 262, 111–120.

Prudlo, J., Bißbort, C., Glass, A., Grossmann, A., Hauenstein, K., Benecke, R., Teipel, S.J., 2012. White matter pathology in ALS and lower motor neuron ALS variants: a diffusion tensor imaging study using tract-based spatial statistics. J. Neurol. 259 (9), 1848–1859.

Puls, I., Jonnakuty, C., LaMonte, B.H., Holzbaur, E.L.F., Tokito, M., Mann, E., Floeter, M. K., Bidus, K., Drayna, D., Oh, S.J., Brown, R.H., Ludlow, C.L., Fischbeck, K.H., 2003. Mutant dynactin in motor neuron disease. Nat. Genet. 33 (4), 455–456.

Richmond, S.B., Fling, B.W., 2019. Transcallosal control of bilateral actions. Exerc. Sport Sci. Rev. 47, 251–257.

Sasaki, S., Maruyama, S., 1992. Increase in diameter of the axonal initial segment is an early change in amyotrophic lateral sclerosis. J. Neurol. Sci. 110 (1-2), 114–120.

Schuster, C., Elamin, M., Hardiman, O., Bede, P., 2016. The segmental diffusivity profile of amyotrophic lateral sclerosis associated white matter degeneration. Eur. J. Neurol. 23 (8), 1361–1371.

Smith, M.C., 1960. Nerve fibre degeneration in the brain in amyotrophic lateral sclerosis. J. Neurol. Neurosurg. Psychiatry 23 (4), 269–282.

Smith, S.M., Jenkinson, M., Johansen-Berg, H., Rueckert, D., Nichols, T.E., Mackay, C.E., Watkins, K.E., Ciccarelli, O., Cader, M.Z., Matthews, P.M., Behrens, T.E.J., 2006. Tract-based spatial statistics: voxelwise analysis of multi-subject diffusion data. Neuroimage 31 (4), 1487–1505.

Tabesh, A., Jensen, J.H., Ardekani, B.A., Helpern, J.A., 2011. Estimation of tensors and tensor-derived measures in diffusional kurtosis imaging. Magn. Reson. Med. 65 (3), 823–836.

Verheijen, M.H.G., Peviani, M., Hendricusdottir, R., Bell, E.M., Lammens, M., Smit, A.B., Bendotti, C., van Minnen, J., Gillingwater, T.H., 2014. Increased axonal ribosome numbers is an early event in the pathogenesis of amyotrophic lateral sclerosis. PLoS One 9 (1), e87255. https://doi.org/10.1371/journal.pone.0087255.

Verstraete, E., Veldink, J.H., Mandl, R.C.W., van den Berg, L.H., van den Heuvel, M.P., He, Y., 2011. Impaired structural motor connectome in amyotrophic lateral sclerosis. PLoS One 6 (9), e24239. https://doi.org/10.1371/journal.pone.0024239.

Welniarz, Q., Dusart, I., Roze, E., 2017. The corticospinal tract: evolution, development, and human disorders. Dev. Neurobiol. 77, 810–829.

Wen, J., Zhang, H., Alexander, D.C., Durrleman, S., Routier, A., Rinaldi, D., Houot, M., Couratier, P., Hannequin, D., Pasquier, F., Zhang, J., Colliot, O., Le Ber, I., Bertrand, A., 2019. Neurite density is reduced in the presymptomatic phase of C9orf72 disease. J. Neurol. Neurosurg. Psychiatry 90 (4), 387–394.

Xie, S., Chen, L., Zuo, N., Jiang, T., 2016. DiffusionKit: a light one-stop solution for diffusion MRI data analysis. J. Neurosci. Methods 273, 107–119.

Yamauchi, H., Fukuyama, H., Ouchi, Y., Nagahama, Y., Kimura, J., Asato, R., Konishi, J., 1995. Corpus callosum atrophy in amyotrophic lateral sclerosis. J. Neurol. Sci. 134 (1-2), 189–196.

Yan, X., Zhou, M., Ying, L., Liu, W., Yang, G., Wu, D., Zhou, Y., Peterson, B.S., Xu, D., 2014. A fast schema for parameter estimation in diffusion kurtosis imaging. Comput. Med. Imaging Graph. 38 (6), 469–480.

Zhang, F., Chen, G., He, M., Dai, J., Shang, H., Gong, Q., Jia, Z., 2018. Altered white matter microarchitecture in amyotrophic lateral sclerosis: a voxel-based meta-analysis of diffusion tensor imaging. Neuroimage Clin. 19, 122–129.

Zhang, H., Schneider, T., Wheeler-Kingshott, C.A., Alexander, D.C., 2012. NODDI: practical in vivo neurite orientation dispersion and density imaging of the human brain. Neuroimage 61 (4), 1000–1016.